Tom Zhang[1]
Department of Mechanical Engineering,
Columbia University,
New York, NY 10027
e-mail: tz2386@columbia.edu

Yubin Liu
Department of Mechanical Engineering,
Columbia University,
New York, NY 10027
e-mail: yl3954@columbia.edu

Nathan Ashmore
Materials & Manufacturing Tech,
Boeing Research & Technology,
Berkeley, MO 63134
e-mail: nathan.a.ashmore@boeing.com

Wayne Li
Boeing Company,
Philadelphia, PA, 19078
e-mail: wayne.w.li@boeing.com

Y. Lawrence Yao
Department of Mechanical Engineering,
Columbia University,
New York, NY 10027
e-mail: yly1@columbia.edu

Effect of Laser Forming on the Energy Absorbing Behavior of Metal Foams

Metal foam is light in weight and exhibits an excellent impact-absorbing capability. Laser forming has emerged as a promising process in shaping metal foam plates into desired geometry. While the feasibility and shaping mechanism has been studied, the effect of the laser forming process on the mechanical properties and the energy-absorbing behavior in particular of the formed foam parts has not been well understood. This study comparatively investigated such effect on as-received and laser-formed closed-cell aluminum alloy foam. In quasi-static compression tests, attention paid to the changes in the elastic region. Imperfections near the laser-irradiated surface were closely examined and used to help elucidate the similarities and differences in as-received and laser-formed specimens. Similarly, from the impact tests, differences in deformation and specific energy absorption were focused on, while relative density distribution and evolution of foam specimens were numerically investigated. [DOI: 10.1115/1.4051285]

Keywords: laser forming, metal foam, impact tests, energy absorption, relative density, advanced materials and processing, laser processes, modeling and simulation, nontraditional manufacturing processes, sheet and tube metal forming

1 Introduction

Metal foam is a lightweight material with a porous structure. With its high strength-to-weight ratio and exceeding impact and energy-absorbing capability, metal foam offers potential applications in the automotive and aerospace industry to serve as crush boxes, airplane noses, and protective casings [1]. These engineering applications often require intricate geometries of the material. Near-net-shaping technology such as three-dimensional (3D)-printing and powder metallurgy can directly produce metal foam in the desired geometry. However, the former suffers from time consumption and small production volume, and the latter is suitable for moderate part sizes and requires molds and thus is limited to large production volume [2,3]. Metal foam are more readily available in generic shapes such as blocks or plates, and further machined or formed into the desired shape. However, mechanical cutting processes such as milling and sawing can cause damage and deformation to cell structures at the cutting surface [1,4]. Spark machining technology like wire electrical discharge machining (wire EDM) is able to minimize cell damage while maintaining a high geometrical accuracy, but, like other material subtraction processes, cannot avoid material waste [5]. Forming processes yield less material waste, but conventional bending process can cause fracture and cell collapse of the material even at low bending angles [6]. Hydroforming can be performed at elevated temperature but causes densification and requires a sandwich setup as protection [7].

Laser forming, which uses thermally induced stress to bend material from generic shapes, has been demonstrated to be able to achieve a high bending angle for metal foam plate without causing excessive cell structure damage and densification [8]. In recent years, a number of studies have been conducted on the laser bending of metal foams. Quadrini et al. [9] and Guglielmotti et al. [10] studied the laser forming of open-cell aluminum foam and aluminum foam sandwich panels and showed the feasibility of bending the material under different laser powers, scanning speeds, and sheet thicknesses. Santo et al. [11] studied the microstructure of open-cell aluminum foam under laser forming and observed grain refinements in the heat affected zone. Localized melting was also observed but did not affect overall bending efficiency. Bucher et al. [8,12] performed an experimental study of the heat transfer and mechanical response of closed-cell Al-foam under laser forming and proposed numerical models of different geometrical accuracies. A modified temperature gradient mechanism was proposed for the bending of foam material, where the foam bends partially due to cell wall bending and crushing near laser-irradiated region. The effect of micro-cracks and cell wall crushing on the crushability of the foam were determined to be insignificant using the J-integral method and foam densification analysis. Despite the efforts spent to understand laser forming of metal foams, the focus of most studies was on the bending angle and bending mechanism. Defects caused by laser forming were observed, but the study of their effects on the crushability of metal foam remains not well understood and lacks experimental validation. To evaluate the effects of laser forming on the energy-absorbing ability of metal foam, it is crucial to understand the compressive behavior of metal foams.

In fact, various studies have been conducted to study the compressive behavior of metal foam without laser forming. In uniaxial compression, metal foam demonstrates a general stress–strain behavior with three distinctive regions: a linear region where stress grows proportionally with strain, followed by a plateau region where stress remains the same while cell collapses, and eventually into a densification region where stress grows exponentially. Jang Kyriakides [13] conducted quasi-static compression on open-cell aluminum foam and discovered that cell crushing in compression started at weakest sites and covers full-cross section of the specimen, forming a crush band. Further crush bands develop either adjacent or separated from the first crush band. The plateau stress was found to be increasing with increasing foam density. Similar

[1]Corresponding author.

Manuscript received January 7, 2021; final manuscript received May 20, 2021; published online July 1, 2021. Assoc. Editor: Gary J. Cheng.

crushing behavior is observed by Bastawros et al. on a closed-cell aluminum alloy foam [14].

In addition to quasi-static compression, several studies have also been conducted on the compressive behavior of metal foam under dynamic loading. Barnes et al. [15] conducted direct impact tests on open-cell aluminum foams and observed that at sufficiently high impact speed, the compression of metal foams enters a shock regime, where the crushing of cell starts from the loading end and gradually develop toward the other end. Deshpande and Fleck carried out split Hopkinson pressure bar (SHPB) and direct impact tests on both closed- and open-cell aluminum foam at strain rate $10^{-3}\ s^{-1}$ to $5000\ s^{-1}$ and observed no clear stress enhancement and change of mode of cell collapse compared to the quasi-static compression at the tested speed [16]. Raj et al. observed an increase of plateau stress of closed-cell foam with increasing strain rate under SHPB experiments, which contradicts Deshpande and Fleck's results. According to Raj et al., this discrepancy is related to the foam manufacturing methods, where mixing blowing agents with liquid melt will cause the foam to be rate sensitive, while foams prepared with other methods tend to be rate insensitive [17]. Ramachandra et al. conducted flat-end punch and spherical-end punch indentation test on closed-cell Alporas foam and studied the energy-absorbing ability of foam at impact velocity from 3 to 30 m/s. A higher energy per deformed volume was observed for impact speed where shockwave effects became significant, and the indentation tests showed a higher energy-absorbing ability compared to uniaxial compression due to tearing and shearing of cell walls [18]. Despite the extensive study on the dynamic compressive behavior of metal foam, the aforementioned studies use as-received material and did not take into account the localized defects and densifications that can emerge from shaping processes. To better understand the mechanical behavior of metal foams in possible applications, it is necessary to evaluate the energy-absorbing ability of metal foam with shaping processes such as laser forming.

The current study focuses on the compressive behavior of closed-cell aluminum foam before and after laser forming. Uniaxial quasi-static compression tests were performed to investigate the stress–strain response and energy-absorbing ability of closed-cell aluminum foam. To simulate the crushing of metal foam in car crashes, dynamic impact tests were also conducted using a modified Charpy impact test to study the energy-absorbing ability of laser-formed metal foam under different impact velocities. The cell surface and cell structure after impact were investigated optically to study the effect of laser forming and impact speeds on the energy-absorbing ability of metal foam. Numerical models with equivalent solid material properties were developed for both compression and impact tests and validated by experimental results.

2 Background

2.1 Metal Foam Mechanical Behavior. Compared to solid material, metal foam exhibits a distinctive compressive behavior. Under quasi-static loading, metal foam typically undergoes three or four characteristic stages of deformation. A typical stress–strain curve from a uniaxial compression test is shown in Fig. 1. Initially, cell structure bends elastically, represented by a linear region in the stress–strain curve. As compression continues, some foam with brittle material properties undergoes an additional collapsing stage, where the weakest layers of cell start to yield and buckle, causing a stress drop in the stress–strain curve [19]. Further loading causes continuous cell structure yielding and collapsing. During this stage, the stress fluctuates slightly around a constant value, known as plateau stress. The collapsing of cells starts to form localized crush bands at discrete locations. After most cell wall collapsing occurs, the foam is compressed to the densification strain, where stress increases exponentially upon further loading and the foam continuously densifies. Due to a wide plateau region in the stress– strain response, metal foam shows excellent energy absorption capability under compressive loading.

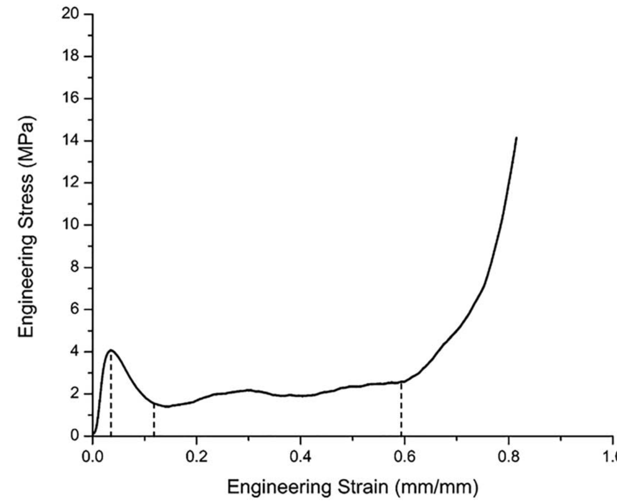

Fig. 1 A typical stress–strain curve from static compression tests. Foam materials demonstrate four distinctive stages during deformation: an initial elastic region, a collapsing region, a plateau region with progressive cell collapsing, and a densification region.

Due to its crushability, metal foam can yield in compression under both hydrostatic and deviatoric stresses. The initial yield surface of metal foam is in elliptical shape in the Von Mises effective stress ($\sigma_e = \sqrt{(3/2)\sigma'_{ij}\sigma'_{ij}}$, prime denotes the deviatoric component) and mean stress ($\sigma_m = (1/3)\ \sigma_{kk}$) space, as shown in Fig. 2.

An isotropic model is proposed by Deshpande and Fleck [20] assuming the yield strength of metal foam is identical in compression and tension. The yield surface is defined by a yield function

$$F = \sqrt{\frac{1}{1+(\alpha/3)^2}(\sigma_e^2 + \alpha^2\sigma_m^2)} - Y \le 0 \tag{1}$$

where Y is the uniaxial yield strength, and α defines the aspect ratio of the yield surface and is related to the plastic Poisson's ratio ν^p via

$$\nu^p = \frac{(1/2) - (\alpha/3)^2}{1+(\alpha/3)^2} \tag{2}$$

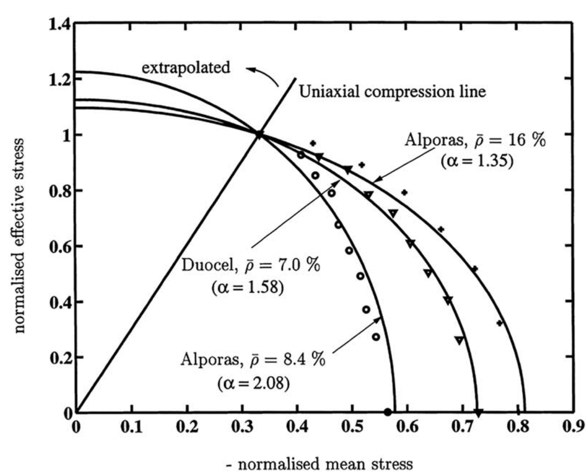

Fig. 2 Initial yield surface of Alporas (closed cell), and Duocel (open cell) foams. Stresses are normalized based on their uniaxial yield strength. $\bar{\rho}$ represents the relative density and α represents the aspect ratio of the yield surface. Only the first quadrant is shown. The yield surface is symmetric about the effective stress axis [20].

When the yield function is positive, the material starts to deform plastically based on the flow rule

$$\dot{\varepsilon}^p_{ij} = \frac{\dot{Y}}{H}\frac{\partial \mathrm{F}}{\partial \sigma_{ij}} \tag{3}$$

where $\dot{\varepsilon}^p_{ij}$ is the plastic strain rate component and H is the hardening modulus obeying the following relation:

$$H = \frac{\sigma_e}{\hat{\sigma}} h_\sigma + \left(1 - \frac{\sigma_e}{\hat{\sigma}}\right) h_p \tag{4}$$

where $\hat{\sigma}$ is the equivalent stress defined as the first term in the yield function F in Eq. (1). h_σ and h_p are the tangent moduli under uniaxial and hydrostatic compression, respectively.

The above model assumes hardening yield in an isotropic manner, which is acceptable for proportional stressing. However, metallic foams develop anisotropy at large plastic strain [20]. In such a case, a kinematic hardening model is needed.

A volumetric hardening model assumes the tensile strength of the metal foam is fixed, while the compressive strength evolves with volumetric strain. A yield function is given as follows:

$$F = \sqrt{\sigma_e^2 + \alpha^2\left(\sigma_m - \frac{p_c + p_t}{2}\right)^2} - \alpha\frac{p_c - p_t}{2} \le 0 \tag{5}$$

where α represent the aspect ratio of the yield surface. p_c and p_t represents the yield strength of the material in compression and tension, respectively.

The flow potential is defined as

$$G = \sqrt{\sigma_e^2 + \frac{9}{2}\sigma_m^2} \tag{6}$$

and obeys the flow rule

$$\dot{\varepsilon}^p_{ij} = \sqrt{2/3}\,\dot{\varepsilon}^p_{ij,axial}\frac{\partial \mathrm{G}}{\partial \sigma_{ij}} \tag{7}$$

where $\dot{\varepsilon}^p_{ij}$ is the plastic strain rate, and $\dot{\varepsilon}^p_{ij,axial}$ is the axial plastic strain rate.

2.2 Metal Foam Under Dynamic Loading. The use of metal foam as an energy absorber will often involve impact accidents in which the loading rate is much higher than the quasi-static loading rate. A strain rate of $\sim 10^2$ to $\sim 10^3\ \mathrm{s}^{-1}$ is often seen in automobile accidents [3]. Based on the loading strain rate, the dynamic compression of metal foam can be classified into two regimes: transitional dynamic and shock.

In the transitional dynamic regime, the macroscopic force balance is maintained, and the crushing behavior of cell structure is similar to quasi-static compression, where cells collapse forming crush bands at discrete locations. However, due to the higher strain rate, stress enhancement is expected for several reasons. First, due to cell wall bending and buckling, transverse motions of the cell structure occur under axial loading. The micro-inertia of the cell wall resists the acceleration in the transverse direction when the metal foam is compressed at high speed, causing an initial axial compression of the cell struts and consequently causing stress enhancement. Second, closed-cell metal foam contains entrapped gas pores. At high impact speed, the entrapped gas has limited time to escape from the micro-cracks and void in the cell walls, which results in the pressurization of the gas and an increase of the overall compressive stress. Despite the reasons that may cause the metal foam to harden at high strain rates, contradicting experimental results were observed regarding the rate sensitivity of metal foam. In Deshpande and Fleck's experiments, no clear stress enhancement is seen up to a strain rate of $5000\ \mathrm{s}^{-1}$. According to their analysis, the quasi-static bending mode is maintained for common commercial foams and micro-inertial plays little role in increasing the compressive strength of the foam. Entrapped gas

Fig. 3 Typical (*a*) as-received metal foam and (*b*) laser-bent specimen (35 × 100 × 10 mm). Laser forming is able to bend the foam specimen to a large bending angle without causing excessive damage to the structural integrity of the metal foam.

contributes to a stress enhancement of less than 1.5% of the quasi-static strength, much less than the scatter band of metal foam property [20].

In a dynamic impact test, when the impact speed is high enough, a shockwave can form at the impact end and travel to the opposite end. In such case, a stress and velocity jump exists at the shockwave front, where the material in front of the shockwave reaches the plateau stress, materials behind the shockwave reached the densification strain and travels at the speed of the shockwave. Assuming a one-dimensional (1D) rigid-plastic behavior, the stress enhancement due to the shockwave effect is as follows [21]:

$$\sigma_d = \sigma_{pl} + \frac{\rho_0 v^2}{\varepsilon_d} \tag{8}$$

where σ_d represents the enhanced dynamic plateau stress, σ_{pl} and ε_d are the plateau stress and densification strain in quasi-static compression, respectively. ρ_0 is the foam density, and v is the impact speed.

According to Deshpande and Fleck, in order for shockwave effect to be dominant, the stress enhancement needs to be at least 20% to exceed the random scatter of material property of metal foam [20]. For the foam used in this study, $\rho_0 = 270\ \mathrm{kg/m^3}$, $\varepsilon_d = 0.8$, and $\sigma_{pl} = 2$ MPa. A critical impact speed around 40 m/s is needed to reach the shock regime, which is higher than the speed in most automobile applications. The loading speed in this study fell in the transitional dynamic regime, and no shockwave effect was observed.

2.3 Numerical Simulation. Numerical simulations were conducted to simulate the quasi-static compression and dynamic impact behavior of metal foam. Foam geometry is simulated as an equivalent homogeneous solid following one of the constitutive behaviors mentioned in Sec. 2.1. The original model and equivalent material properties of the foam were adopted from the study of Bucher et al. [8]. Uniaxial stress–strain data were extracted from experiments in this study. The collapsing of cell structure is reflected as the increase of relative density, which is calculated based on volumetric strain. In uniaxial compression and impact testing, large plastic deformation occurs; thus, the volumetric hardening model was used. All simulations were conducted in ABAQUS.

For quasi-static compression simulation, a displacement-controlled loading platen was applied on a cylindrical foam specimen 0.5 mm/min. The loading and fixed back support platen were defined as a rigid surface with a friction coefficient of 0.61. The lateral surface of the specimen is not confined. For impact simulation, a cylindrical foam specimen is fixed on a rigid surface and hit with a rigid mass on the other ends at specified speeds. The lateral surface of the foam specimen is confined. Friction was considered between the loading mass and the foam specimen with a friction coefficient of 0.61. An axisymmetric mesh with linear stress elements C3D8 and C3D6 was used for both quasi-static compression and impact simulation.

2.4 Laser Forming of Metal Foam. Laser forming is a thermal–mechanical process that uses a laser to scan along a path to induce bending of a workpiece. It has been well studied for solid material and has also proven its feasibility in bending metal foams, as shown in Fig. 3. The bending mechanism of metal foam is mostly assumed to be the temperature gradient mechanism (TGM) originally proposed by Geiger and Vollertsen for solid material [22]. It applies to the condition where a large temperature gradient is present between the top and bottom of a workpiece. When the laser is irradiated on the workpiece, the irradiated spot heats up rapidly and tries to expand, but due to the localized heating of the laser, the surrounding material remains cold and confines the expansion of the material, resulting in the plastic compression of the laser-scanned path. When the material cools down the laser-heated region ended up shorter in the direction perpendicular to the laser scanning direction due to the plastic compressive strain, causing the workpiece to bend toward the laser. Bucher et al. proposed a modified temperature gradient mechanism (MTGM) to explain the laser bending of metal foam [8]. MTGM suggests that while most of TGM still applies to laser forming of metal foam, the bending is not mainly caused by plastic compressive strain but also by the slight cell wall bending and collapsing. The bending and collapsing of the cell wall cause densification of the material over the top surface and shifts down the neutral axis of the workpiece, which limits the tensile deformation at the bottom surface.

In addition to the cell wall deformation during the bending process, laser forming also introduces other structural imperfections to metal foams. According to Bucher et al. [8] melting at thin walls, although rare, was observed starting from the first laser scan and progressive melting developed upon further scans. Micro-cracks also form at the bottom surface due to naturally occurring stress concentrations and grew larger as the bending angle increases. Even though the overall structural integrity of the metal foam is not significantly disturbed by these localized micro-defects, how does these defects affect the foam's compressive behavior and energy-absorbing ability need to be investigated.

3 Experimental Procedures

A closed-cell Al-foam with 7 wt% silicon, a volume fraction of 11%, and a density of 280 kg/m^3 was used in this study. The average cell size ranges from 3 to 4 mm. The foam was manufactured by melt-foaming method which uses TiH_2 as a foaming agent and calcium to increase the viscosity of the liquid metal. The foam blocks were first cut with a slitting saw to a length of 100 mm and a width of 35 mm to perform laser forming. The height of the specimen was 10 mm for compression test specimens to make the laser forming effect more significant for the overall specimen, and 30 mm for impact test specimens to allow the foam specimen to absorb more impact energy. Laser forming experiments were conducted with a 90-W CO_2 laser with a spot size of 12 mm and a scanning speed of 5 mm/s in order to generate temperature gradient across the thickness of the specimen without causing excessive melting at the laser-irradiated surface. A radial scanning pattern was designed to provide increase the laser-affected area and make the laser-forming effect more uniform, as shown in Fig. 4. Successive scans were placed far apart, and the specimen

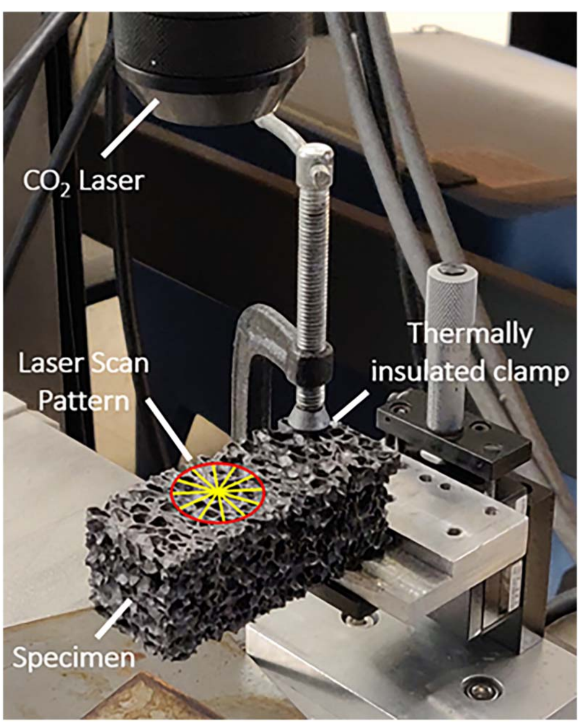

Fig. 4 Laser forming to prepare for compression and impact testing specimens. Foam block shown is 35 mm wide, 100 mm long, and 30 mm thick. A 34-mm diameter circular region was irradiated with CO_2 laser at 90 W and a beam spot size of 12 mm, in 6 straight laser scans at 5 mm/s. Laser-treated region was then cut with wire EDM to a cylindrical shape with a diameter of 25 mm and a height of 30 mm. Specimens for compression tests were similarly prepared, with an original 35 × 100 × 10 mm foam block and a final specimen 30 mm diameter and 10 mm high.

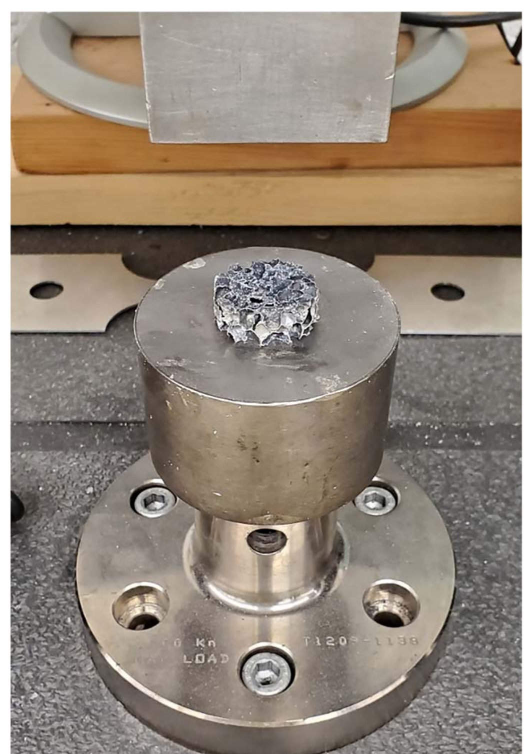

Fig. 5 Quasi-static compression test conducted on a material testing machine. The specimen shown is 30 mm in diameter and 10 mm in height before testing.

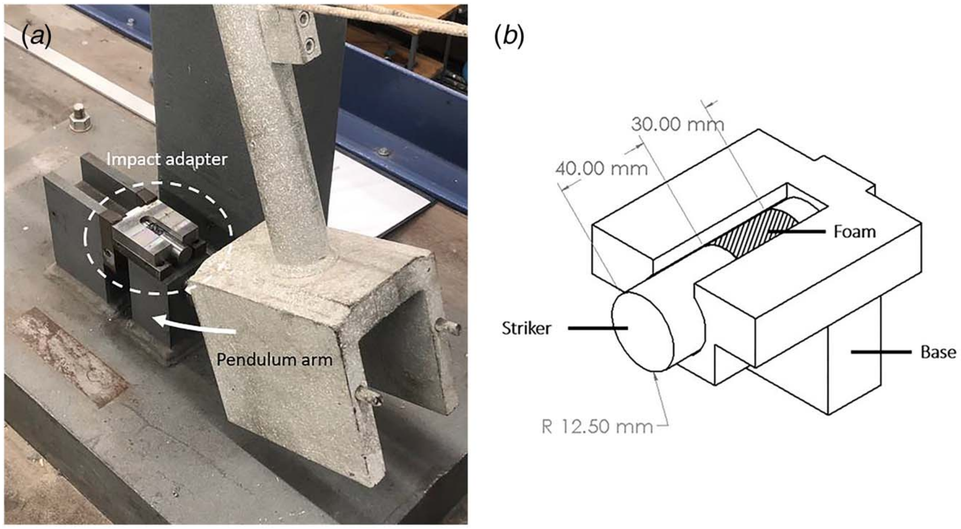

Fig. 6 (***a***) **The Charpy impact tester and** (***b***) **impact adapter for the Charpy impact tester. The pendulum arm of the Charpy tester was released from fixed heights and came into contact with the striker and compressed the foam specimen. A 25-mm diameter and 30-mm high foam specimen is placed inside the adaptor, with direct contact between the moving striker and a fixed back support. The adaptor is set in the slot of the Charpy test machine.**

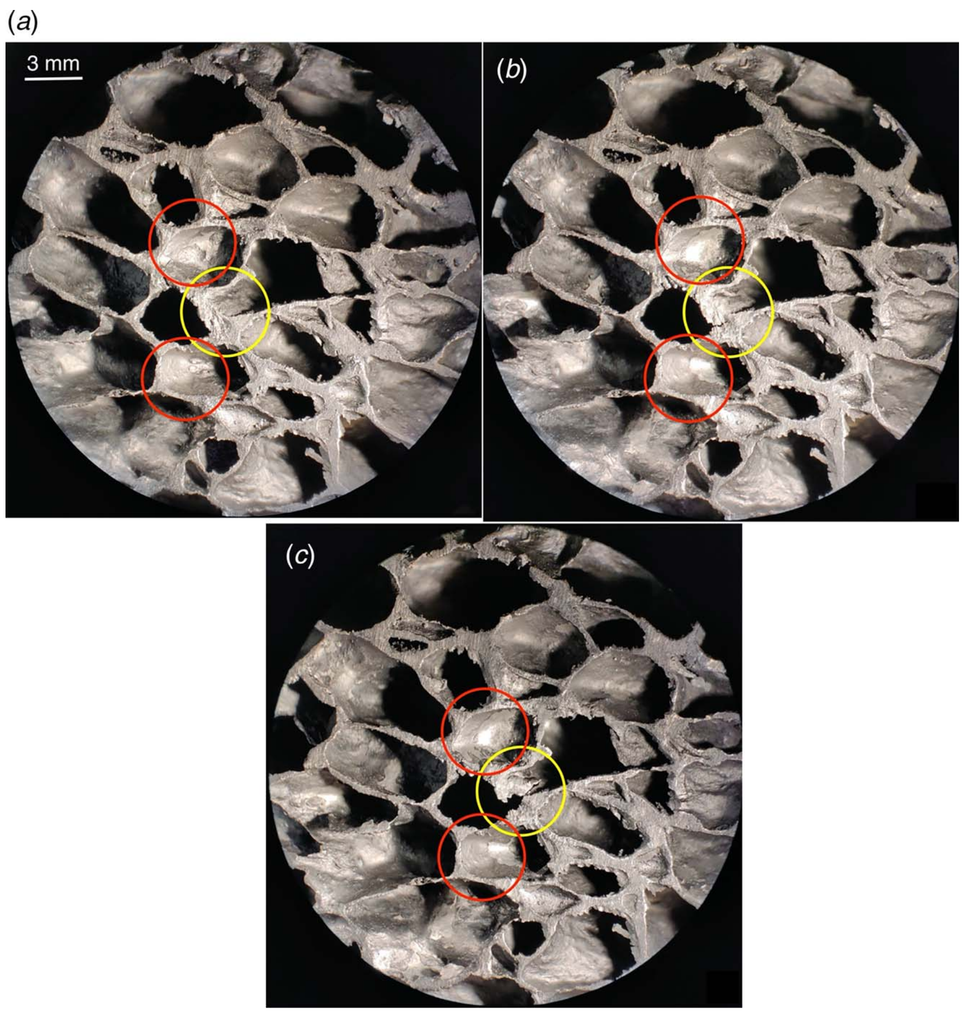

Fig. 7 **The surface of foam specimen affected laser scans,** (***a***) **after 1 scan,** (***b***) **after 5 scans, and** (***c***) **after 10 scans at a laser power of 90 W and a scanning speed of 5 mm/s. As highlighted in the center, a crack initiated and propagated at a cell wall. The cell wall surface also underwent partial melting starting from the first laser scan. Further development of the melting with additional laser scans was not observed. The cell wall crack and surface melting weaken the structure at the laser-treated surface but remain localized.**

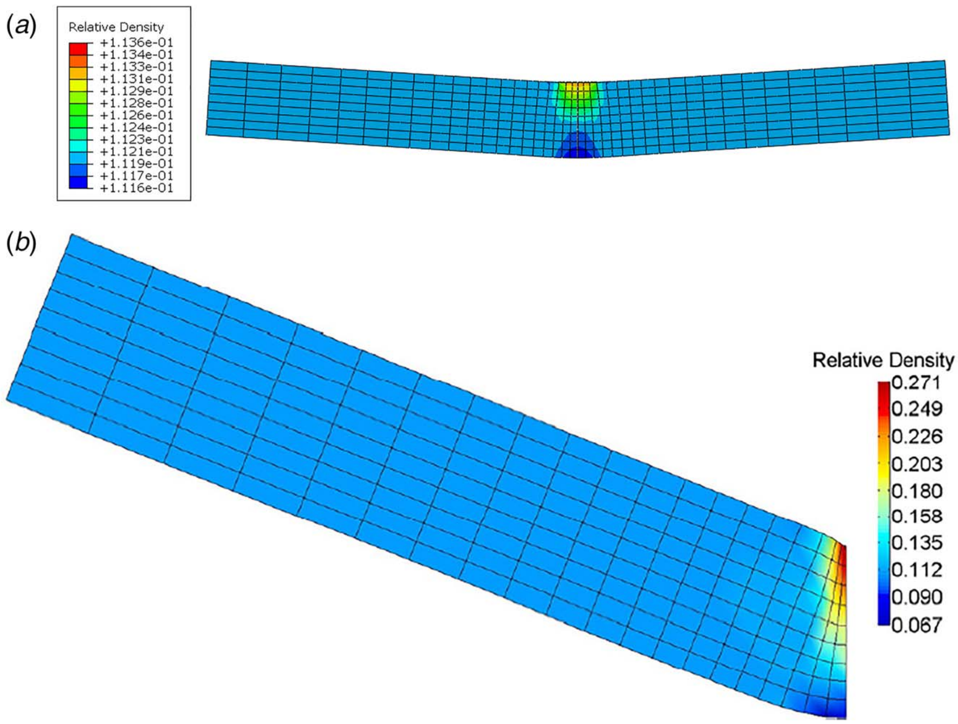

Fig. 8 Relative density distribution (*a*) after being scanned once with laser 90 W and 5 mm/s with a spot size of 12 mm. Deformation is magnified by 20 times. Relative density refers to the ratio of the overall foam density versus the density of the solid makeup of the cell wall. After a single scan, the increase in density near the bending axis is less than 2%. At the bottom surface, the foam expands due to tensile strain developed during laser forming, and (*b*) after repeated scanned with laser at 180 W and 10 mm/s with a spot size of 12 mm until reaching a bending angle of 45 deg [8]. Maximum foam density reaches 0.271, where further compression requires an exponential increase in compressive stress. Foam crushability is sacrificed by only over the top half of the foam and the width of the densified region is limited to half of the laser spot size.

was cooled with an air jet in between scans to reduce heat accumulation. Repeated sets of scans were applied on both compression and impact specimens. The compression test specimens were laser treated on one side, while the impact test specimens were treated on both sides to increase the laser-affected region on the larger specimen. During laser forming, graphite was applied to the foam surface to increase laser absorption. Optical microscopy was used to capture the laser-treated surface after each radial scan. After laser scanning, the foam specimens were cut into cylindrical shapes using wire EDM to minimize cell wall damage in the cutting process and to minimize mechanical cutting-induced stress. The specimens for the compression test had a diameter of 30 mm and a height of 10 mm, while the specimens for impact testing had a diameter of 25 mm and a height of 30 mm.

Quasi-static compression test was conducted according to standard ASTM C365/C365M-16 on an Instron 5569a test machine (Fig. 5). Graphite powder was applied to the compression platens to reduce friction. Each sample was preloaded to 45N and compressed at 0.5 mm/min until it reached a compression force of 20 kN. Engineering stress–strain data were then calculated from the crosshead displacement and compression force data from the test machine.

Impact test was conducted on a Charpy test machine with an adjusted sample adaptor shown in Fig. 6(*a*). The standard Charpy impact test is designed to test material's notch toughness or ductile-brittle transformation temperature, where a pendulum arm is released from fixed heights and impacts a notched specimen. The specimen is fractured from the impact, and the fracture behavior or the fracture energy is then examined. For the current study, an adaptor (Fig. 6(*b*)) with the foam specimen was fixed in place of the original Charpy test sample, to allow the foam specimen to receive axial impact from the pendulum arm and fully bring the pendulum arm to stop from the impact. The adaptor was made from low-carbon steel with significantly higher strength and stiffness than the foam to ensure minimal deformation and energy absorption of the adaptor. The striker ensures the pendulum force is more uniformly applied to the cylindrical foam specimen. The impact velocity upon the contact between the pendulum arm and the striker was calculated based on the release height and conservation of energy (ignoring friction). Laser-treated and as-received foam specimens were impacted at various arm release heights, and the final length of each specimen was measured after the pendulum arm came to rest.

4 Results and Discussion

4.1 Minor Imperfections Resulting From Laser Forming. Laser forming of metal foams mainly utilizes heat-induced plastic deformation to bend the material into the desired shape, whereas minor cell wall crushing also contributes to the bending. However, this process also induces structural imperfections in the material. These imperfections may hamper the energy-absorbing ability of metal foam and are worth investigating. These imperfections occur only at the laser-irradiated surfaces, that is, the end surfaces of the cylindrical specimen.

The first imperfection caused by laser forming is the cell wall crushing as the foam bends. As explained in Sec. 2.4, the temperature gradient during the laser forming process causes the laser affected region to be plastically compressed, resulting in the cell wall bending and collapsing near the laser-scanned area. Microcracks can also form during this process. Figure 7 shows such

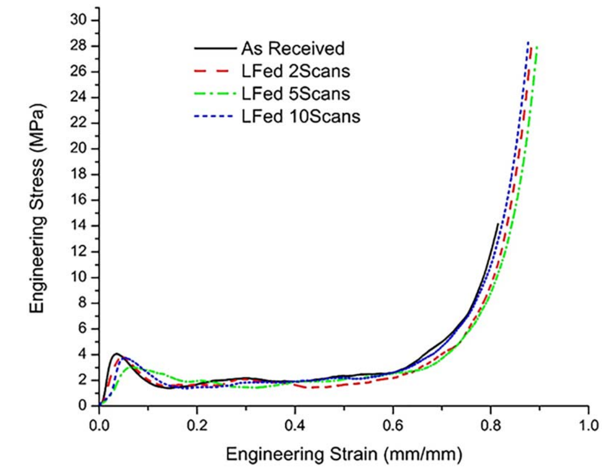

Fig. 9 Comparison of stress–strain behavior of metal foam before and after laser forming from quasi-static compression tests. They all exhibit distinctive stress–strain behavior of metal foam materials. While laser-formed specimens showed similar plateau stresses and strain at densification as an un-laser-formed specimen, laser-formed samples underwent an initial ductile region before elastic compression, possibly caused by the yielding of the weakened surface structure during laser forming.

crack of the cell wall in laser-irradiated area highlighted in the center. After the first scan, the wall remained intact (Fig. 7(*a*)). After five scans, a visible crack was formed (Fig. 7(*b*)). After 10 laser scans, the crack propagated and weakened the entire cell wall (Fig. 7(*c*)). Another imperfection induced in the laser forming process is cell wall partial melting at the laser-treated region. The laser power used in this study is selected to be low to avoid melting of the cell wall and limit large bending of the foam specimen to create a more stable test condition for compression and impact testing. But even at a laser power as low as 90 W, the cell wall surfaces highlighted in Fig. 7 started to partially melt from the first laser scan (Fig. 7(*a*)) but the melting did not further develop much when the number of scans increased. This is likely due to the fact that, after the first melting, laser intensity may have reduced somewhat because the distance between the wall and the laser focal plane may have changed. The cell wall surface crack and melting can disrupt the structural integrity of the foam

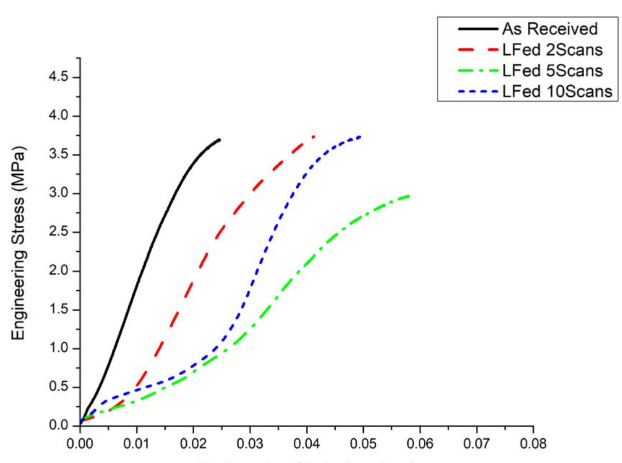

Fig. 10 Stress–strain curves up to collapse stress extracted from Fig. 9. Samples with a higher scan number show an initial ductile region, caused by the surface damage and crack initiation in the sample during laser forming.

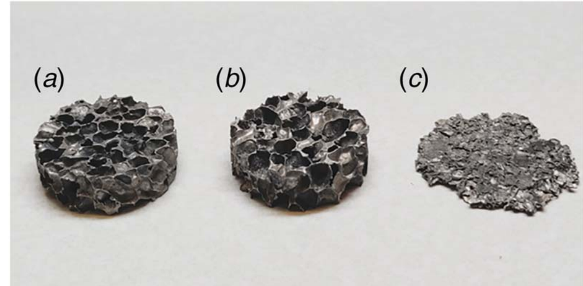

Fig. 11 Cylindrical samples for compression tests. (*a*) As received, (*b*) radially scanned 10 times at laser power of 90 W and scanning speed of 5 mm/s with a beam spot size of 12 mm, and (*c*) statically compressed sample at compression speed of 0.5 mm/min and up to compression force of 20 kN. All samples are 30 mm in diameter and 10 mm high.

structure at the laser-treated region and thus creating a localized weak spot. When the foam is under compression or impact, the cell wall collapsing will be more likely to initiate from the laser-treated surface. However, the cracks and surface melting remain isolated and only happen near the laser-treated surface, thus only have a limited effect on the overall energy-absorbing ability of the foam.

As part of the bending mechanism, cell wall crushing and melting is unavoidable in the bending process and causes foam densification at the bending axis thus reducing the crushability of the foam, especially at high bending angle. Simulation results help assess the extent of the densification of metal foam during laser forming. A single scan of laser at 90 W and 5 mm/s was conducted on a foam specimen with dimension 100 mm × 35 mm × 10 mm, with a spot size of 12 mm. A half of the cross section (due to symmetry) perpendicular to the scanning direction is shown in Fig. 8(*a*). After the single scan, the relative density of the foam increases locally at the bending axis, from a 0.112 base value to a maximum of 0.114. At low bending angles, laser forming only cause very minor densification of the foam, and the overall structural integrity and crushability of the foam are maintained. However, as more laser scans are conducted, the foam further densifies as the bending angle increases. According to a similar simulation conducted by Bucher et al., [8] at a bending angle of 45 deg, the relative density of the foam can reach 0.271 (Fig. 8(*b*)). While still far from a solid density ($R = 1$), the foam becomes very resistant to deformation after reaching a relative density of 0.2, requiring the compressive stress to increase exponentially to further deform the material and thus sacrificing the foam's crushability. However, densification resulted from laser forming can also be beneficial when the treated foam is subjected to bending, as the densified material can withstand more compressive stress before yielding during the bending of the material. In addition, the densified region is highly localized. As can be seen in both simulations, the densified region spans half the thickness of the foam and is only about half of the laser spot size wide. At the bottom surface, the material is even less dense than the rest of the material due to the tensile strain developed during laser forming, allowing the material to be able to withstand more compression before reaching a densified state. Thus, the overall crushability of foam is mostly maintained during laser forming.

4.2 Quasi-Static Compression Test. Quasi-static tests were conducted on both laser-formed and as-received foam specimens and four representative stress–strain curves are shown in Fig. 9. A laser power of 90 W and a scanning speed of 5 mm/s were used as representative process parameters to limit melting while still able to create a temperature gradient across the specimen. Several conclusions can be drawn from the quasi-static compression results. First, laser-formed specimens demonstrate similar plateau stress and

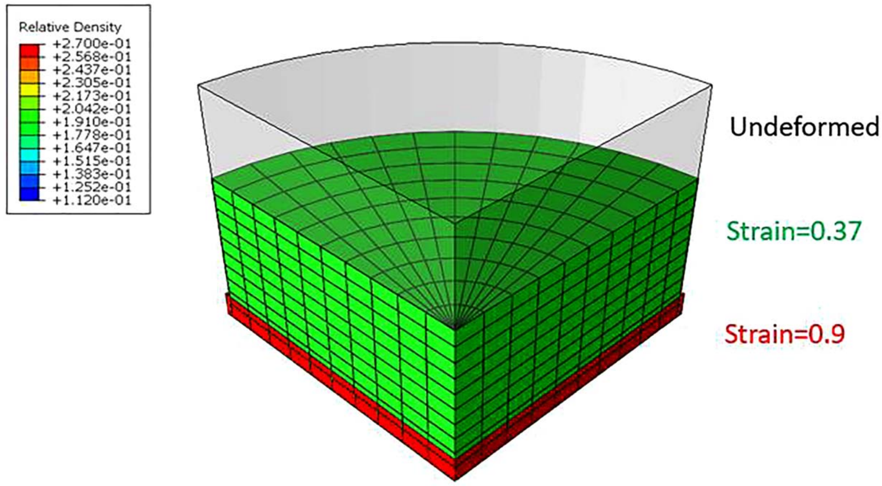

Fig. 12 Relative density evolution during quasi-static compression of the foam, where the relative density of the foam is homogeneous. As the uniaxial strain increases, the relative density of the foam increases. Shown is a quarter specimen with 15 mm in radius and10 mm in height.

densification strain with the as-received foam specimens. Since the bending angle of the specimen is controlled to be small, there is no significant densification of the foam, and the original foam plateau stress and densification strain are maintained during the laser forming process and does not show a trend as the number of laser scans increases. This shows that the imperfections induced in the laser forming process do not have a significant effect on the foaming property beyond the elastic region.

Another phenomenon that can be observed is the difference in the elastic region. It appears the laser-formed sample is more ductile than the as-received sample. However, when taking a closer look, the laser-formed specimens showed an initial ductile region, followed by another elastic region, as shown in Fig. 10. The initial ductile region extends as the number of laser scan increases. The cell wall cracks and surface melting during the laser forming process weakens the structure at laser-treated region. Due to the localized disruption of the structural integrity, the laser-treated region tends to yield at a lower stress than the rest of the structure, thus creating an initial ductile region before the rest of the material getting elastically compressed. Young's modulus of the laser-formed specimens and the as-received specimens are comparable and fall in the scatter band of metal foam properties. Therefore, after laser forming, the quasi-static compressive response of metal foam remains largely the same, but with an additional ductile region before the elastic compression. When considering the specific energy absorption of the foam, which is calculated by the area under the stress–strain curve up to densification strain, the laser-formed sample demonstrated a slight reduction in energy absorption, especially when the number of laser scans is large. For the specimens tested, the largest specific energy absorption reduction is below 13%, which still falls in the random scatter band of foam properties.

Typical quasi-static compression of metal foam involves the formation of discrete and localized crush bands that spreads the cross section of the metal foam specimen. In this study, in order to make the laser-affected region more dominant over the entire specimen, the height of the specimen was chosen to be 10 mm, about two to 3 cells in the axial direction. Under such dimension, there are not enough cells in the axial direction to form a characteristic crush band, instead, the bending and crushing of cell wall happened uniformly, and no distinguishing crushing behavior is observed for laser-formed specimens and as-received specimens. Figure 11 shows a comparison between the as-received, laser-treated, and compressed foam specimen. After compression, the diameter of the foam specimen is increased by about 13%, and the relative density of the foam increases from 0.11 to 0.3 after reaching the compression force limit. The experimental observation is consistent with simulation results (Fig. 12). At this state, the cell structure is fully collapsed in the axial direction and further compression requires an exponential increase in the compressive stress. However, the foam is still far from a solid relative density of 1. This is due to the fact that axial compression cannot fully compact the material and the material still maintains a porous structure.

4.3 Dynamic Compression Test. While quasi-static compression gives insight into how the foam behaves under compressive loading, the use of metal foam often involves impact events where quasi-static behavior may not apply. The modified Charpy impact test was conducted to study the foam's response when impacted with a mass with known impact velocity. In order to allow the foam specimen to fully absorb the kinetic energy of the

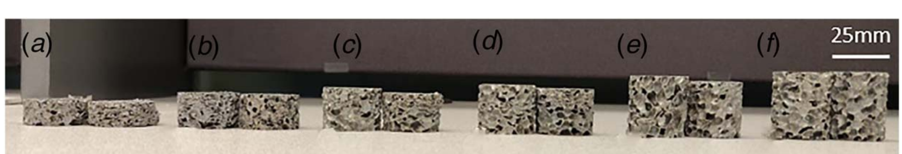

Fig. 13 Cylindrical sample after modified Charpy impact testing with impact speed (*a*) $v = 1.22$ m/s, (*b*) $v = 1.10$ m/s, (*c*) $v = 0.97$ m/s, (*d*) $v = 0.83$ m/s, (*e*) $v = 0.66$ m/s, and (*f*) before impact. For each group, the specimen on left is as received, while the specimen on right is scanned with CO_2 laser at 90 W and 5 mm/s, repeated 10 times on each end. Laser-formed specimen experienced moderately larger deformation due to its surface weakening from laser treatment.

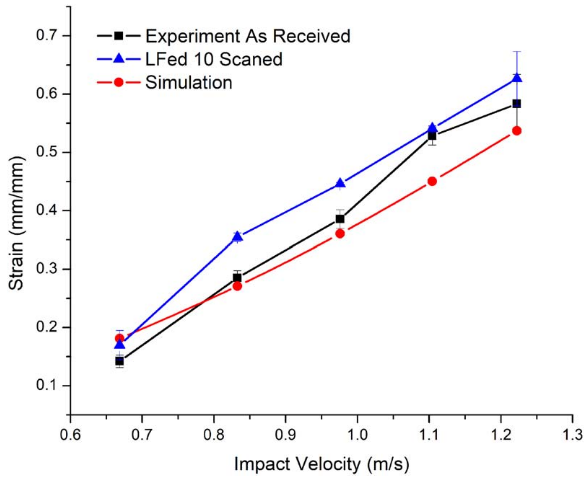

Fig. 14 Strain after impact at different impact velocities. The laser-treated specimens demonstrate a moderately larger final strain after impact compared to as-received specimens. This is caused by the weakening effect of the surface damage during the laser forming process. Simulation results overall slightly underestimate the deformation during impact; this is due to the over accounting of inertial effect in the dynamic analysis, which is not dominant at the impact speeds tested. Error bars represent standard deviation.

pendulum arm, the height of the foam specimen was extended to be 30 mm. Foam specimens treated with laser on both ends, as well as untreated specimens, were impacted at five different impact speeds, ranging from 0.67 m/s to 1.22 m/s. As mentioned in Sec. 2.2, at this impact speed, the shockwave effect is not dominant, and the behavior of metal foam falls in the transitional dynamic regime, which is the case for most automotive applications.

The representative laser-formed and as-received specimens after impact is shown in Fig. 13. And the strain after impact is plotted against impact velocity in Fig. 14. As the impact speed increases, more cell structure collapses to absorb the increased kinetic energy; thus, more deformation is seen at a higher impact speed. Due to the pendulum arm of the Charpy tester having a much greater mass than the foam specimen, the foam structure is fully collapsed even at impact speed as low as 1.22 m/s. However, in any

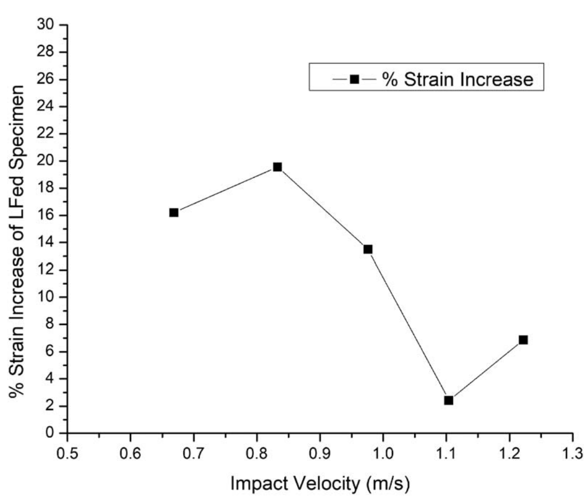

Fig. 15 Increase of impact-induced strain at different impact velocities. The specimen, laser forming condition, and impact test conditions are the same as in Figs. 13 and 14. The increase is smaller at higher impact velocities likely due to the dominance of mechanical impact at these velocities.

potential applications of the foam, the mass of the foam and the impact area will be much greater, and thus, the foam will be able to endure a much higher impact speed. Once the foam is fully compressed, further increasing the impact speed creates only minimal deformation as the cell structure is fully collapsed and further compression only compacts the material.

When considering the effect of laser forming, the laser-treated specimen showed a moderately larger deformation compared to the as-received specimen, as seen in both Figs. 13 and 14. This is related to the weakening effects from laser forming process. The micro-cracks and partial melting at laser-treated region makes the foam more susceptible to cell wall collapsing thus reducing the strength of the material. The percentage strain increase of laser-formed specimens compared with as-received metal foam is shown in Fig. 15 with different impact velocities. They range from about 2 to 20%, with smaller increases at higher impact velocities. This is likely due to the fact that the effect of mechanical impact at these velocities overshadows the effect of laser forming. The simulation results of as-received metal foam shown in Fig. 14 largely follow the experimental trend. They overall slightly underestimate the deformation during impact likely due to the over accounting of inertial effect in the dynamic analysis, making the foam more resistant to deformation, which the inertial effect is less dominant in the impact speed range tested.

This weakening effect can also be seen from the crush behavior of the foam specimen. Figure 16 shows the cross section of the foam specimens after impact testing. Characteristic crush band highlighted within white boundaries can be seen for impact speed up to 0.97 m/s. For as-received specimens, the crush band locations were random and depend on the weakest structure in the foam. Laser-treated specimens have localized weak spots at the laser-irradiated surface (top surface) due to the micro-cracks and surface melting developed during laser forming. The weakened structure there is more susceptible to cell wall crushing and thus serves as an initiation spot for the crush band development, thus the initial crush band of the laser-treated specimens all has their crush band close to the impact end (top surface). Once the impact speed is high enough, the crush band can no longer be distinguished and crushing appears to be uniform across the entire specimen, as observed for impact speed 1.10 m/s and 1.22 m/s.

Figure 17 shows the relative density of a quarter foam specimen after impact velocity of 0.67 m/s, 0.97 m/s, and 1.22 m/s, respectively. Since explicit cell structure is not modeled in the homogeneous model, the crushing behavior of the metal foam is represented in an average sense. The crush band formation is not seen, and the relative density is more or less uniform throughout the specimen, especially at lower impact velocities. Figure 18 shows simulation results of the time history of relative density during impact at an initial impact velocity of 1.22 m/s. All points including three on the impacted top surface (radius = 0, 6.25, and 12.5 mm) and three along the centerline of the cylindrical specimen (impacted top surface, mid-surface, and back-surface) show uniform densification from 11% (as received) to about 25%. The rise is linear initially and levels off toward the end. This is consistent with the fact that the chosen impact velocities translate to the transitional dynamic regime, in which no shock phenomenon exists.

Another phenomenon worth investigating is the energy absorption during the impact testing. The pendulum arm impacts the striker and is brought to a stop, and the kinetic energy of the pendulum arm is absorbed during the impact event. While friction exists between the specimen and the slot, the energy dissipated during the impact can be neglected since the slot surface was well lubricated with graphite powder, and the foam cannot withstand high normal stress from the slot surface before collapsing. Simulation results show that using a typical kinematic friction coefficient between aluminum and steel yield a friction dissipation less than 2% of the total kinetic energy in all simulated impact speeds. The deformation of the fixture and striker are also assumed to be negligible due to their stiffness being much higher than the foam. Therefore, the kinetic energy of the pendulum arm is assumed to be fully absorbed

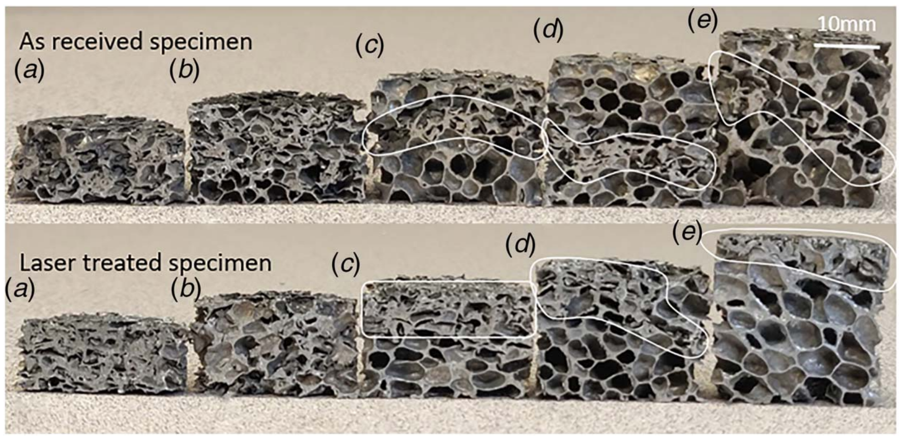

Fig. 16 Crush band development after impact from the top surface at speed of (*a*) $v=1.22$ m/s, (*b*) $v=1.10$ m/s, (*c*) $v=0.97$ m/s, (*d*) $v=0.83$ m/s, and (*e*) $v=0.66$ m/s. Crushing of foam specimens starting from the collapsing of the weakest structure. After the cell collapse, it causes stress concentration on other cell walls in the same layer and causes collapsing to develop a crush band. Laser-formed specimens tend to develop a crush band from the laser-treated impact surface, while the crush band location of as-received samples are more random and depend on where the weakest cell structure is.

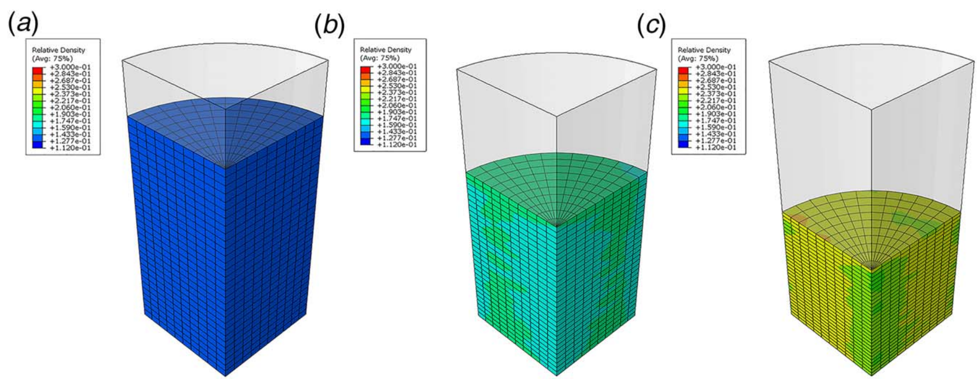

Fig. 17 Relative density distribution after impacted from the top at impact speed of (*a*) 0.67 m/s, (*b*) 0.97 m/s, and (*c*) 1.22 m/s. Deformation factor is set to 1, and grey body represents undeformed specimen. The relative density is more or less uniform throughout the specimen especially at lower impact velocities. As indicated in Sec. 2.2, none of the velocities induce a shockwave effect.

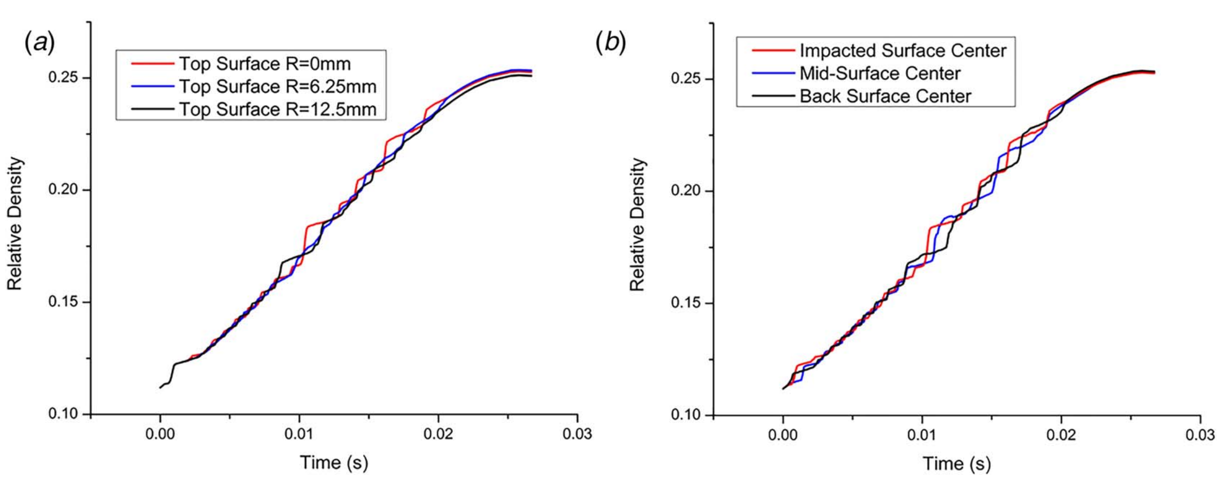

Fig. 18 Time history of relative density during impact test at a velocity of 1.22 m/s as predicated by simulation: (*a*) three locations on the impacted top surface and (*b*) three locations along the centerline of the cylindrical specimen. They all show uniform densification from 11.2% to about 25%, initially linearly before leveling off.

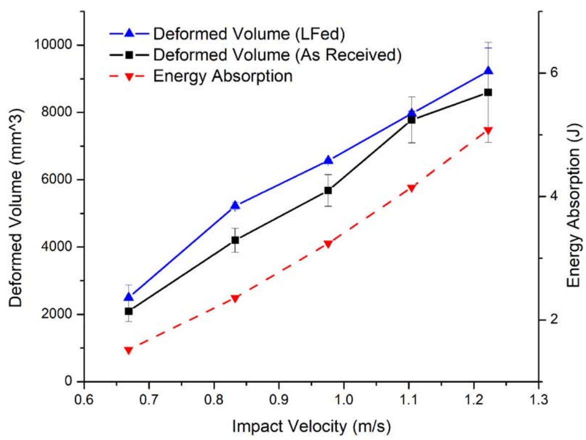

Fig. 19 As the impact velocity increases, the impact creates more deformation on the foam. The foam also absorbs a higher kinetic energy during the impact. As a result, the specific energy absorption of the foam fluctuates over a constant value. Error bars represent standard deviation.

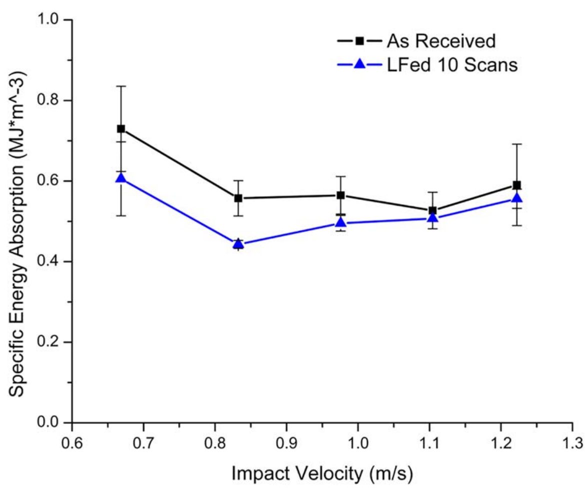

Fig. 20 Specific energy absorption at different impact speeds. Laser-formed specimen shows a slight decrease in energy-absorbing ability than as-received specimen due to the surface imperfections. Rate hardening is not obvious due to the low-density foam used and low testing speed. Error bars represent standard deviation.

by the foam material. The energy so absorbed during impact tests is shown in Fig. 19 for different impact velocities. Shown in the same figure are deformed volume, similar to strain, of as-received foam and foam after 10 laser scans, respectively. As discussed earlier, foam after forming deformed slightly more than as-received foam primarily because of the forming-induced structural imperfections at the laser-irradiated region.

The specific energy absorption of the foam is evaluated by the total kinetic energy absorption over the deformed volume, and the result is shown in Fig. 20. As the impact speed increases, the specific energy absorption hobbles around a constant level. This means no rate of hardening is observed in the experiments. Normally stress enhancement is expected in closed-cell foam in the transitional dynamic regime due to micro-inertia effect and entrapped gas as mentioned in Sec. 2.2. However, due to the low relative density of the foam and a low testing speed, these stress enhancement effects are negligible.

When comparing the laser-formed and as-received specimen, due to the surface imperfections caused during the laser forming process, the laser-formed specimen is locally weakened at the treated surface and undergoes more deformation while absorbing the same amount of kinetic energy. Such properties are undesirable in the application as the foam can absorb less impact energy before reaching the fully dense state and put laser-formed foam at a slight disadvantage in specific energy absorption compared with the as-received foam material. However, all the reduction in specific energy falls within the 20% scatter in foam material properties, and at almost all impact speeds, the specific energy absorption standard deviation shows the overlap between the laser-formed and as-received specimen. Therefore, laser forming does negatively impact the behavior of the foam in impact-absorbing ability, but not significantly.

5 Conclusion

The laser forming process has a few undesirable effects, although very minor and localized, on the mechanical properties of aluminum alloy foam under the conditions investigated. Micro-cracks and cell wall partial melting were observed via optical microscopy in the laser-irradiated region. The slightly reduced structural integrity caused by these defects explains the slightly reduced specific impact energy absorption quantified from the impact tests. Crush bands in as-received specimens tend to be more randomly located, while those in laser-formed specimens tend to locate near the laser-irradiated surface due to the same reason. In the quasi-static compression tests, the laser-formed specimens demonstrate similar plateau stress and densification strain as the as-received foam specimens, while exhibiting a small ductile region preceding the elastic deformation. This phenomenon is attributed to the immediate collapsing of particularly weakened cells before the rest of the material gets elastically compressed. Overall, laser forming is a viable process in shaping metal foam.

Acknowledgment

The financial support from the National Science Foundation under a GOALI Grant No. CMMI-1725980 is gratefully acknowledged. Thanks to Professors C. Chen and M. Zhang of Soochow University, China, for making metal foam materials available.

Conflict of Interest

There are no conflicts of interest.

Data Availability Statement

The data sets generated and supporting the findings of this article are obtainable from the corresponding author upon reasonable request.

References

[1] Ashby, M. F., Evans, A. G., Fleck, N. A., Gibson, L. J., Hutchinson, J. W., and Wadley, H. N. G., 2000, *Metal Foams: A Design Guide*, Elsevier, New York.
[2] Kennedy, A., 2012, *Powder Metallurgy, Porous Metals and Metal Foams Made From Powders*, InTech, Rijeka, Croatia, Chap. 2.
[3] Claar, T. D., Yu, C. J., Hall, I., Banhart, J., Baumeister, J., and Seeliger, W., 2000, "Ultra-lightweight Aluminum Foam Materials for Automotive Applications," SAE Paper No. 2000-01-0335.
[4] Qiao, H., Murthy, T. G., and Saldana, C., 2019, "Structure and Deformation of Gradient Metal Foams Produced by Machining," ASME J. Manuf. Sci. Eng., **141**(7), p. 071009.
[5] Martin Matz, A., Kammerer, D., Jost, N., and Oßwald, K., 2016, "Machining of Metal Foams With Varying Mesostructure Using Wire EDM," Procedia CIRP, **42**, pp. 263–267.
[6] D'Urso, G., and Maccarini, G., 2011, "The Formability of Aluminum Foam Sandwich Panels," Int. J. Mater. Form., **5**(3), pp. 243–257.
[7] Mansoor, B., Nassar, H., Shunmugasamy, V. C., and Khraisheh, M. K., 2015, "Three Dimensional Forming of Compressed Open-Cell Metallic Foams at Elevated Temperatures," Mater. Sci. Eng. A, **628**, pp. 433–441.

[8] Bucher, T., Young, A., Zhang, M., Chen, C. J., and Yao, Y. L., 2018, "Thermally Induced Mechanical Response of Metal Foam During Laser Forming," ASME J. Manuf. Sci. Eng., **140**(4), p. 041004.

[9] Quadrini, F., Guglielmotti, A., Squeo, E. A., and Tagliaferri, V., 2010, "Laser Forming of Open-Cell Aluminium Foams," J. Mater. Process. Technol., **210**(11), pp. 1517–1522.

[10] Guglielmotti, A., Quadrini, F., Squeo, E. A., and Tagliaferri, V., 2009, "Laser Bending of Aluminum Foam Sandwich Panels," Adv. Eng. Mater., **11**(11), pp. 902–906.

[11] Santo, L., Bellisario, D., Rovatti, L., and Quadrini, F., 2012, "Microstructural Modification of Laser- Bent Open-Cell Aluminum Foams," Key Eng. Mater., **504–506**, pp. 1213–1218.

[12] Bucher, T., Bolger, C., Zhang, M., Chen, C., and Yao, Y. L., 2016, "Effect of Geometrical Modeling on the Prediction of Laser-Induced Heat Transfer in Metal Foam," ASME J. Manuf. Sci. Eng., **138**(12), p. 121008.

[13] Jang, W.-Y., and Kyriakides, S., 2009, "On the Crushing of Aluminum Open-Cell Foams: Part II Analysis," Int. J. Solids Struct., **46**(3–4), pp. 635–650.

[14] Bastawros, A.-F., Bart-Smith, H., and Evans, A. G., 2000, "Experimental Analysis of Deformation Mechanisms in a Closed-Cell Aluminum Alloy Foam," J. Mech. Phys. Solids, **48**(2), pp. 301–322.

[15] Barnes, A. T., Ravi-Chandar, K., Kyriakides, S., and Gaitanaros, S., 2014, "Dynamic Crushing of Aluminum Foams: Part I—Experiments," Int. J. Solids Struct., **51**(9), pp. 1631–1645.

[16] Deshpande, V. S., and Fleck, N. A., 2000, "High Strain Rate Compressive Behaviour of Aluminium Alloy Foams," Int. J. Impact Eng., **24**(3), pp. 277–298.

[17] Raj, E., Parameswaran, V., and Daniel, B. S. S., 2009, "Comparison of Quasi-Static and Dynamic Compression Behavior of Closed-Cell Aluminum Foam," Mater. Sci. Eng. A, **526**(1–2), pp. 11–15.

[18] Ramachandra, S., Sudheer Kumar, P., and Ramamurty, U., 2003, "Impact Energy Absorption in an Al Foam at Low Velocities," Scr. Mater., **49**(8), pp. 741–745.

[19] Peroni, M., Solomos, G., and Pizzinato, V., 2013, "Impact Behaviour Testing of Alumnium Foam," Int. J. Impact Eng., **53**, pp. 74–83.

[20] Deshpande, V., and Fleck, N., 2000, "Isotropic Constitutive Models for Metallic Foams," J. Mech. Phys. Solids, **48**(6–7), pp. 1253–1283.

[21] Reid, S. R., and Peng, C., 1997, "Dynamic Uniaxial Crushing of Wood," Int. J. Impact Eng., **19**(5–6), pp. 531–570.

[22] Geiger, M., and Vollertsen, F., 1993, "The Mechanisms of Laser Forming," CIRP Ann., **42**(1), pp. 301–304.